



This is a repository copy of *Quantitative histomorphometry of capillary microstructure in deep white matter*.

White Rose Research Online URL for this paper:  
<http://eprints.whiterose.ac.uk/146227/>

Version: Published Version

---

**Article:**

Mozumder, M., Pozo, J.M., Coelho, S. et al. (5 more authors) (2019) Quantitative histomorphometry of capillary microstructure in deep white matter. *NeuroImage: Clinical*, 23. 101839. ISSN 2213-1582

<https://doi.org/10.1016/j.nicl.2019.101839>

---

**Reuse**

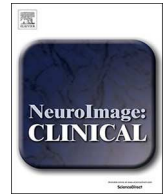
This article is distributed under the terms of the Creative Commons Attribution-NonCommercial-NoDerivs (CC BY-NC-ND) licence. This licence only allows you to download this work and share it with others as long as you credit the authors, but you can't change the article in any way or use it commercially. More information and the full terms of the licence here: <https://creativecommons.org/licenses/>

**Takedown**

If you consider content in White Rose Research Online to be in breach of UK law, please notify us by emailing [eprints@whiterose.ac.uk](mailto:eprints@whiterose.ac.uk) including the URL of the record and the reason for the withdrawal request.



[eprints@whiterose.ac.uk](mailto:eprints@whiterose.ac.uk)  
<https://eprints.whiterose.ac.uk/>



## Quantitative histomorphometry of capillary microstructure in deep white matter

Meghdoot Mozumder<sup>a,b</sup>, Jose M. Pozo<sup>c</sup>, Santiago Coelho<sup>c</sup>, Marina Costantini<sup>a</sup>, Julie Simpson<sup>d</sup>, J. Robin Highley<sup>d</sup>, Paul G. Ince<sup>d</sup>, Alejandro F. Frangi<sup>c,e,\*</sup>

<sup>a</sup> Centre for Computational Imaging & Simulation Technologies in Biomedicine (CISTIB), Department of Electronic and Electrical Engineering, The University of Sheffield, Sheffield, UK

<sup>b</sup> Department of Applied Physics, University of Eastern Finland, P.O. Box 1627, 70211 Kuopio, Finland

<sup>c</sup> Centre for Computational Imaging & Simulation Technologies in Biomedicine (CISTIB), School of Computing and School of Medicine, University of Leeds, UK

<sup>d</sup> Sheffield Institute for Translational Neuroscience (SITraN), The University of Sheffield, Sheffield, UK

<sup>e</sup> LICAMM Leeds Institute of Cardiac and Metabolic Medicine, School of Medicine, University of Leeds, Leeds, UK

### ARTICLE INFO

#### Keywords:

Vascular dementia  
Deep white matter  
Deep subcortical lesion  
Capillary microstructure

### ABSTRACT

White matter lesions represent a major risk factor for dementia in elderly people. Magnetic Resonance Imaging (MRI) studies have demonstrated cerebral blood flow reduction in age-related white matter lesions, indicating that vascular alterations are involved in developing white matter lesions. Hypoperfusion and changes in capillary morphology are generally linked to dementia. However, a quantitative study describing these microvascular alterations in white matter lesions is missing in the literature; most previous microvascular studies being on the cortex. The aim of this work is to identify and quantify capillary microstructural changes involved in the appearance of deep subcortical lesions (DSCL). We characterize the distribution of capillary diameter, thickness, and density in the deep white matter in a population of 75 elderly subjects, stratified into three equal groups according to DSCL: Control (subject without DSCL), Lesion (sample presenting DSCL), and Normal Appearing White Matter (NAWM, the subject presented DSCL but not at the sampled tissue location). Tissue samples were selected from the Cognitive Function and Aging Study (CFAS), a cohort representative of an aging population, from which immunohistochemically-labeled histological images were acquired. To accurately estimate capillary diameters and thicknesses from the 2D histological images, we also introduce a novel semi-automatic method robust to non-perpendicular incidence angle of capillaries into the imaging plane, and to non-circular deformations of capillary cross sections. Subjects with DSCL presented a significant increase in capillary wall thickness, a decrease in the diameter intra-subject variability (but not in the mean), and a decrease in capillary density. No significant difference was observed between controls and NAWM. Both capillary wall thickening and reduction in capillary density contribute to the reduction of cerebral blood flow previously reported for white matter lesions. The obtained distributions provide reliable statistics of capillary microstructure useful to inform the modeling of human cerebral blood flow, for instance to define microcirculation models for their estimation from MRI or to perform realistic cerebral blood flow simulations.

### 1. Introduction

Cerebral white matter lesions (WML) are common in the aging brain, with prevalence of over 90% in over-65 age group (Wharton et al., 2015). WML are associated with dementia, impaired motor function, depression, and Alzheimer's disease (AD) (Barber et al., 1999; DeBette and Markus, 2010). WML may also be a risk factor for mild cognitive impairment progressing into dementia (Devine et al., 2013).

Pathologically, they are associated with glial changes and myelin loss (among others), and are recognized as areas of high signal intensity in  $T_2$ -weighted magnetic resonance imaging (MRI) (Ovbiagele and Saver, 2006). WML may be sub-classified by location into those within the white matter of the centrum semiovale (deep subcortical lesions, DSCL) and periventricular lesions. Each has its own clinical relevance, but both have been associated with small vessel-related vascular pathology (Park et al., 2011). Microvascular changes and hypo perfusion are

\* Corresponding author at: Centre for Computational Imaging & Simulation Technologies in Biomedicine (CISTIB), School of Computing and School of Medicine, University of Leeds, UK.

E-mail address: [a.frangi@leeds.ac.uk](mailto:a.frangi@leeds.ac.uk) (A.F. Frangi).

<https://doi.org/10.1016/j.nicl.2019.101839>

Received 18 December 2018; Received in revised form 4 April 2019; Accepted 24 April 2019

Available online 25 April 2019

2213-1582/ © 2019 The Author(s). Published by Elsevier Inc. This is an open access article under the CC BY-NC-ND license

(<http://creativecommons.org/licenses/by-nc-nd/4.0/>).

intimately involved in the etiopathogenesis of dementia (Thal et al., 2003). Abnormalities have been also found in normal appearing white matter (NAWM) regions in brains with DSCL, such as microglial activation and alterations of a variety of cellular pathways (Wharton et al., 2015), albeit not apparent in  $T_2$ -MRI. This suggests a possible field effect of white matter abnormality within which DSCL arise, implying that NAWM is important for investigation. Perfusion MRI studies have demonstrated low cerebral flow rates in age-related WMLs compared to NAWM (Marstrand et al., 2002; Brickman et al., 2009), indicating reduced cerebral blood flow could lead to development of WMLs. However, the specific vascular morphology changes in deep white matter involved in the appearance of DSCLs have not been studied yet.

Here, we aimed to identify and quantify capillary microstructural changes potentially responsible for cerebral blood flow reduction in DSCLs. We considered samples of deep subcortical white matter from an aged population of 75 subjects (71–100 years) from the Cognitive Function and Aging Study (CFAS), stratified according to age-related DSCL: Control (subject without DSCL), Lesion (sample presenting DSCL), and NAWM (the subject presented DSCL but not in the sampled tissue). From these samples, immunohistochemistry-stained tissue sections and corresponding microscopy images were acquired.

Several approaches to micro vessel characterization using stained tissues exist. Some notable stereological approaches use the disector method (Gundersen et al., 1993) for estimating density of capillary branches, the Cavalieri method (Gundersen and Jensen, 1987) for estimating total volume, and the virtual sphere method (Mouton et al., 2002) for estimating length density of the capillaries. Several studies have been performed to estimate capillary densities and mean length (Løkkegaard et al., 2001; Bouras et al., 2006). Some have led to conflicting results (Richard, 2010), possibly due to variations within the population studied or limitations of the proposed methods. Table 1 summarizes the population, tissue region, studied condition, and relevant associated findings. Most studies focused on the cortex or the hippocampus, and only two in white matter. A qualitative assessment of vascular changes in WMLs (Fernando et al., 2006) reported increase of vascular thickness, no change in internal diameters and no change in capillary density. Quantification of these characteristics from deep white matter regions is missing in the literature.

Mancardi et al. (Mancardi et al., 1980), using light and electron microscopy of stained tissue sections, presented one of the earliest estimations of capillary wall (basement membrane) thickness in AD. Their estimation only considers manually selected capillaries appearing perpendicular to the section. Cassot et al. (Cassot et al., 2006; Lauwers et al., 2008) reported capillary diameters, lengths, and densities, in human brain sections injected with Indian ink and imaged with

confocal laser microscopy. The statistics of capillary diameters reported by Cassot et al. have been used in several capillary flow modeling studies such as (Su et al., 2012). However, the study reports statistics from the cortex of a single subject. This severely limits the generality of the findings to the wider population and to white matter. Two other stereology-based studies (Løkkegaard et al., 2001; Bouras et al., 2006) provided estimates of capillary diameters, mean lengths and densities, in cortex and hippocampus, from 19 and 5 subjects, respectively. These two works used stacks of stained immunohistochemistry slices, and measured diameters from the capillary inner wall to its axis, using an interactive computer software that excluded capillaries with odd shapes, thus restricting the number of capillaries analyzed and potentially biasing results.

The immunohistochemistry-stained tissue sections acquired in this work, unlike the Indian-ink filled capillaries technique in (Cassot et al., 2006), allow imaging larger tissue regions and estimating basement membrane thickness. We quantified the distributions of capillary basement membrane thickness, lumen diameters and capillary densities in each of the three groups (Control, NAWM, and DSCL) and statistically analyzed their differences. To extract the morphological features, we automatically analyzed histological images with a new method robust to the angulation between capillaries and the image plane, and to the non-circularity of their cross-sections. Unlike the method in (Løkkegaard et al., 2001; Bouras et al., 2006), our method allows including most of the present capillaries in the analysis. We validated this method in a set of synthetic capillary images, comparing two alternative versions of it, with different levels of complexity, and an automated version of the method proposed by Mancardi et al. (Mancardi et al., 1980).

## 2. Material and methods

### 2.1. Sample preparation and histology acquisition

Tissue samples for this work came from the Cognitive Function and Aging Study (CFAS) neuropathology cohort (Brayne et al., 2006). Brains were removed with the consent of the next of kin and with multicenter research ethics committee approval, according to standard CFAS protocols (Fernando et al., 2004). The age range of the subjects was 71–101 years. Brains were removed within 60 h of death, one cerebral hemisphere was fixed in buffered formaldehyde and sliced into 10 mm thick coronal slices. These slices were: immediately anterior to the temporal stem, at the level of the pulvinar, and at the posterior most limit of the occipital horn of the lateral ventricle. One slice was chosen per subject. These slices were scanned using  $T_1$  and  $T_2$  weighted MRI

**Table 1**  
Previous studies on cerebral capillary characteristics and their changes in aging and dementia.

Ref.	Region	#Subjects (Age)	Condition	Findings
(Hunziker et al., 1979)	C	34 (19–94)	Aging	Diameter(°)
(Mann et al., 1986)	C	25 (26–96)	Aging AD	Diameter(–), Density(°) Diameter(°), Density(°)
(Mancardi et al., 1980)	C	8 (50–65)	AD	Thickness(°), Tortuosity(°)
(Lepelletier et al., 2017)	C	30 (54–95)	AD	Thickness(°), Collagen fraction(°)
(Farkas et al., 2000)	C	20 (63–87)	AD PD	Thickness(°) Thickness(°)
(Claudio, 1995)	C	5 (n/a)	AD	Thickness(°)
(Bouras et al., 2006)	C,CA1	19 (82–101)	AD	Diameter(°), Density(°)
(Fischer et al., 1990)	C,H	22 (23–92)	AD	Density(°), Tortuosity(°)
(Bell and Ball, 1981)	H	15 (21–94)	Aging AD	Diameter(°), Density(°) Diameter(–), Density(–)
(Farkas et al., 2006)	PWM	14 (40–90)	Aging	Thickness(°), Density(–)
(Fernando et al., 2006)	PWM,DSCL	19 (≥ 65)	Aging	Density(–)

Changes with the mentioned condition are marked as increase (°), decrease (°) or no change (–). Abbreviations: C = cortex, H = hippocampus, PWM = periventricular white matter, PD = Parkinson's disease. Ages are in years.

(more details and example images in (Fernando et al., 2004)). The lesions were diffuse, observed as subtle increased signal intensities in the deep subcortical WM. These diffuse changes were rated by three experienced observers (blind to clinical status) and given a score for DSCL using a modified Scheltens' scale (Scheltens et al., 1993). There was no further available clinical diagnosis of these subjects. Following this scoring, the coronal slices were stored in formalin until required for this study (at least four weeks). Blocks were sampled from the slices and allocated in three groups: CTRL, NAWM, and DSCL. CTRL blocks were taken from cases where all three levels were scored as 0 on this scale or where only one slice had a score of a maximum of 1. DSCL blocks were taken from regions with a Scheltens' score of 4 or greater. NAWM blocks were taken from lesion free regions of deep white matter in which a DSCL of score 3 or greater was present elsewhere. The formalin-fixed blocks of tissue were processed to paraffin and embedded in paraffin wax using conventional protocols (Fernando et al., 2004). For each block, a section of 5  $\mu\text{m}$  thickness was cut for immunohistochemistry (the in plane dimensions of the samples were around 20 mm  $\times$  20 mm). The sections were collected onto charged slides and underwent antigen retrieval with Access Revelation RTU (A. Menarini Diagnostics Ltd., Winnersh, UK) in a pressure cooker at pH 6. Sections were immunostained for collagen IV (a basal lamina marker; Abcam ab6586; 1:500) using an IntelliPATH FLX system (A. Menarini Diagnostics Ltd., Winnersh, UK). Immunohistochemistry was performed using a standard ABC method, visualised with diaminobenzidine tetrachloride (DAB), and the sections counter stained with hematoxylin. Prepared sections were scanned and digitized at 40 $\times$  magnification using a Nanozoomer XR (Hamamatsu, Photonics Ltd. Hertfordshire, UK) in NDPI format (Photonics, 2016). The final resolution of the images was of 0.23  $\mu\text{m}/\text{pix}$ . The high resolution images were extracted from NDPI images using NDPITools (Deroulers et al., 2013). The computations were carried out on a server with Intel(R) Xenon(R) CPU E5-2699 v3 @2.3 GHz and 256GB ram.

## 2.2. Histological image format conversion and processing

Given the size of the image files (around 35 GB each slice), and the computational limitations, NDPIsplit (Deroulers et al., 2013) was used to split the histology images into multiple TIFF tiles of equal dimensions and were loaded separately to MATLAB (R2016a, Mathworks, Natick, MA) to obtain the whole image of each slice. Next, we applied color deconvolution (Ruifrok et al., 2001) to change the representation of the RGB images to DAB, hematoxylin, and background channels. Only the DAB intensities were kept, leaving a single-channel image. Fig. 1 shows a typical DAB-channel image of an immunohistochemistry slice of collagen IV staining. The individual capillary positions were obtained

by an initial manually selected threshold segmentation, followed by the MATLAB clustering algorithm "clusterdata" (Srivastava et al., 2013). Objects with diameters > 10  $\mu\text{m}$  (Løkkegaard et al., 2001; Richard, 2010) (representing larger vessels) and objects consisting of only a few pixels (corresponding to background noise) were discarded. Also, capillaries with zero inner diameters (representing highly tilted capillaries) were discarded. For the DSCL sections, ROIs specific to the area within the lesion, based on the  $T_1$  and  $T_2$  MRI images, were chosen. After individual capillary identification and isolation, the corresponding DAB-channel image patches were used for the morphometric parameters estimation.

## 2.3. Model-based capillary morphometrics from histology

We considered three methods for the estimation of the capillary morphometry, based on models describing the capillary images with increasing complexity and generality.

**Method 1** (Mancardi et al., 1980) assumes all capillaries are approximately normal to the histological section, and hence the inner and outer mean diameters from histology images correspond to actual capillary inner and outer diameters, respectively. To estimate the inner and outer mean radius, we first segmented the gray-scale capillary histological images using Otsu's method (Otsu, 1975). Then, inner and outer boundary points were extracted from the segmented images, and subsequently the mean radii and thickness were calculated.

**Method 2** assumes that capillary histology sections can be modeled as projections of tilted hollow cylinders. The capillaries in each histological image were fit to hollow cylinder models by maximizing the Pearson correlation between the projection images of the synthetic capillary models and the acquired histological images of the capillaries. Pearson correlation was chosen as it has demonstrated sensitivity to object orientations (Foster and Sanderson, 1984). Each tilted hollow cylinder model was parameterized by six parameters,

$$\mathbf{X} = (x_0, y_0, \theta, \phi, r, t) \quad (1)$$

representing its center position  $(x_0, y_0)$ , inclination  $(\theta)$  and azimuthal  $(\phi)$  angles, and inner radii  $(r)$  and thickness  $(t)$ .

To initialize the model parameters, we considered the inner and outer capillary boundary contours extracted from its Otsu's segmentation. The center  $(x_0, y_0)$  was initialized as the centroid of these contours. Each was then fitted to two an ellipse using least-square minimization. The orientation  $(\phi, \theta)$  was initialized as the one in which a circular cylinder produce the outer elliptical boundary as cross section. The radii of the elliptical boundaries along the minor axis of the outer boundary give initial estimates for inner and outer radii. Their difference provides the initial estimate of capillary thickness  $t$ . Finally, the

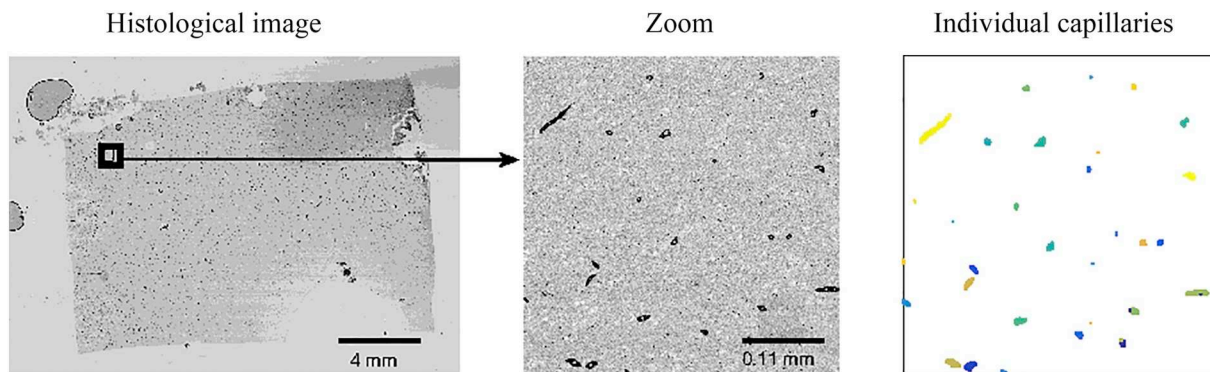


**Fig. 1.** Identification and isolation of capillaries from a typical immunohistochemically-labeled histological image from a brain tissue sample. The tissue sample is from an ex-vivo brain of a female 91 year old, taken from the posterior most limit of the occipital horn of the lateral ventricle. A zoom of the image is shown (middle) with the resulting individual capillaries identified after segmentation (right).

Pearson correlation was maximized by optimizing the parameters using the MATLAB function *fminsearch*, implementing a derivative-free Nelder-Mead simplex search method (Lagarias et al., 1998).

**Method 3** extends Method 2 by considering a hollow cylinder model with irregular cross section described by Fourier coefficients:

$$r(\phi) = \gamma_0 + \sum_{i=1}^N \gamma_{2i} \cos(i\phi) + \sum_{i=1}^N \gamma_{2i-1} \sin(i\phi) \quad (2)$$

with  $\phi \in [0, 2\pi)$  the angular variable and  $2N + 1$  Fourier coefficients  $\gamma_0, \gamma_1, \dots, \gamma_{2N}$ . We selected  $N = 5$  by considering the smallest number of modes that described a set of 2000 boundary shapes extracted from segmented capillary images with a relative mean square error below 5%.

The model was parameterized as.

$$\mathbf{X} = (x_0, y_0, \theta, \phi, \gamma_0, \dots, \gamma_{2N}, t) \quad (3)$$

where  $x_0, y_0, \theta, \phi$ , and  $t$  has the same meaning as in (1). The parameters  $(x_0, y_0, \phi, t)$  were initialized as in Method 2. The parameters  $\gamma_0, \dots, \gamma_{2N}$  were initialized by fitting (2) to the mean irregular radii,  $r(\phi)$  of the extracted inner and outer boundary of the segmented image, considering the capillaries as initially perpendicular,  $\theta = 0$ . The Pearson correlation was maximized also as for Method 2.

#### 2.4. Synthetic histology phantom data: generation and analysis

We synthetically generated 5000 realistic capillary images to evaluate the performances of the different estimation methods. To avoid inverse crime (Kaipio and Somersalo, 2005) (using the same or nearly the same models to synthesis and to invert data in an inverse problem), the generated synthetic images had more realistic properties than considered in the fitting model of Method 3. The synthetically generated cylinders had changes in the inner radii along their major axis. The radius variation was based on variations observed across capillaries within control groups perpendicular to the imaging cross section. Synthetic images were corrupted with spatially-correlated noise modeled as a Gaussian Markov field, with the standard deviation of noise set at 5% of the maximum image intensity. We created a set of 1000 samples of synthetic capillary images with radii and thickness uniformly sampled from the intervals  $r \in [2 \mu\text{m}, 4 \mu\text{m}]$ ,  $t \in [0.2 \mu\text{m}, 3 \mu\text{m}]$ , and orientation homogeneously sampled from the spherical cap with  $\theta \leq 45^\circ$ . Larger orientations were ignored since on average, they appeared with zero inner diameters, being rejected by the cutoff criteria. We defined the target radii from the mean perimeter of the cross sections along the cylinder.

The performances of Methods 1 to 3 were evaluated by analyzing their respective error in estimating diameter and thickness when applied to the synthetic capillary images.

#### 2.5. Histological image analysis and capillary morphometry

The individual capillaries obtained from histology data, were fit using Method 3 (since it provided the best performance) to estimate diameter and thickness for the different samples.

We also measured the capillary density, defined as the number of capillaries per unit area, following the same definition as most previous works (Farkas et al., 2000; Fischer et al., 1990; Bell and Ball, 1981). We also computed the collagen area fraction (fraction of stained pixels in the image), since some works used it as a measure of density (Lepelletier et al., 2017). For each group, the statistics of all investigated variables were analyzed. MATLAB codes used to analyze the histology data, and the original and modeled capillaries from the 75 subjects are available at (Mozumder, 2018).

### 3. Results

#### 3.1. Performance evaluation of histomorphometric analysis

The result of fitting each of the three considered models to an individual capillary image is illustrated in Fig. 2 (more examples in Supplementary Fig. 2). To evaluate the performances of these methods, we synthetically generated capillary images with more realistic properties than the ones considered in the models. The estimation errors for capillary orientation, diameter, and thickness from these synthetic images are shown in Fig. 3 for the three methods. The error distributions are presented as *violin plots* (Hoffmann, 2015) to make evident any skewness. Given the non-normality of these distributions (assessed by the Kolmogorov-Smirnov test (Massey, 1951)), the Wilcoxon rank sum test (Gibbons and Chakraborti, 2011) was applied to evaluate their differences. Methods 2 and 3 outperform Method 1, providing similar errors for orientation and thickness. Although Method 3 is more complex, and hence susceptible to over-fitting the image noise, it is superior to Method 2 in estimating capillary diameters. Further complex models were not considered, since the obtained errors were smaller than the expected changes in these capillary parameters, reported on similar vascular pathologies (Bouras et al. (Bouras et al., 2006) reported around 30% decrease in diameters in AD, Farkas et al. (Farkas et al., 2000) reported around 100% increase in thickness in aging and AD subjects). The average computation times for the model fitting to each single capillary image, were 0.1 s, 15.7 s, and 86.3 s, for Methods 1, 2, and 3, respectively.

#### 3.2. Statistical distribution of capillary features

The lumen diameter and basement membrane (BM) thickness from each capillary of all 75 subjects were estimated using Method 3, which showed the smaller error on the evaluation. The distribution of lumen diameter and BM thickness of individual capillaries along the CTRL, NAWM and DSCL groups are shown in Fig. 4. This includes intra- and inter-subject variability. Fig. 5 shows the distribution of subject-specific means and intra-subject standard deviations of diameter and thickness for each group. The distribution of subject-specific capillary density and collagen area fraction are also shown. The mean capillary thickness increases in DSCL compared to NAWM ( $p = 0.05$ , Wilcoxon rank sum test). No significant change is observed in mean lumen diameters. However, the intra-subject standard deviation of the diameters is lower in DSCL compared to CTRL ( $p = 8 \times 10^{-5}$ ) and NAWM ( $p = 7.5 \times 10^{-5}$ ). This suggests a reduction in the capillaries with most extreme diameters (highest and/or lowest). In agreement, capillary density is reduced for DSCL compared to CTRL ( $p = 0.02$ ) and to NAWM ( $p = 0.03$ ). Parameter statistics were plotted as box-plots since the number of samples was lower (25 samples per group). The computation time in analyzing each subject (file conversion, segmentation, clustering etc. as described in *Material and methods*, followed by capillary model fitting) was around 96 h on a MATLAB implementation.

### 4. Discussion

In recent years there has been growing evidence indicating that microcirculation impairment and capillary dysfunction are linked to developing DSCLs in the elderly (Marstrand et al., 2002; Brickman et al., 2009). The aim of this study was to investigate the specific microstructural changes in capillaries related to DSCL. Those changes can lead to microcirculation impairment, being an important factor in developing DSCLs in the elderly. There exist several studies investigating brain capillary features in similar pathologies or conditions (see Table 1). However, most only focus on the cortex or the hippocampus, and none on the deep white matter. The work by Cassot et al. (Cassot et al., 2006; Lauwers et al., 2008), for instance, was based on a single brain from the Duvernoy database (Duvernoy et al., 1981) with subjects

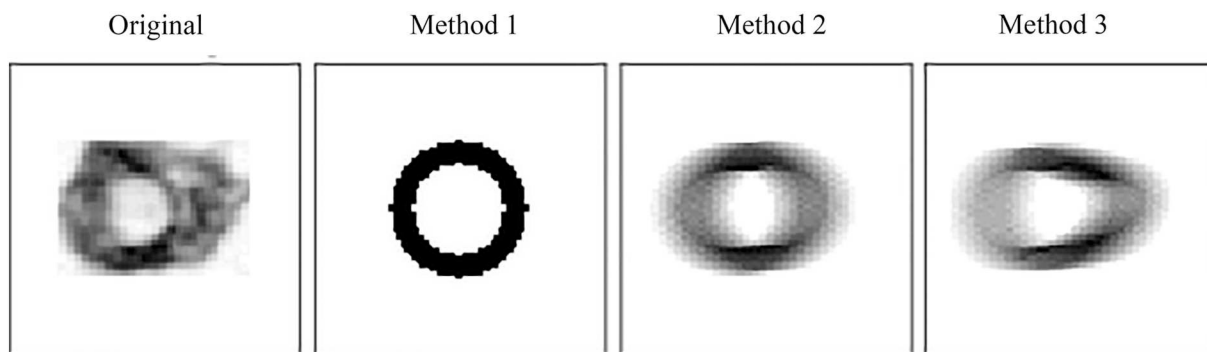


Fig. 2. Example of the original image of one capillary and the corresponding fitting obtained by each of the three tested methods.

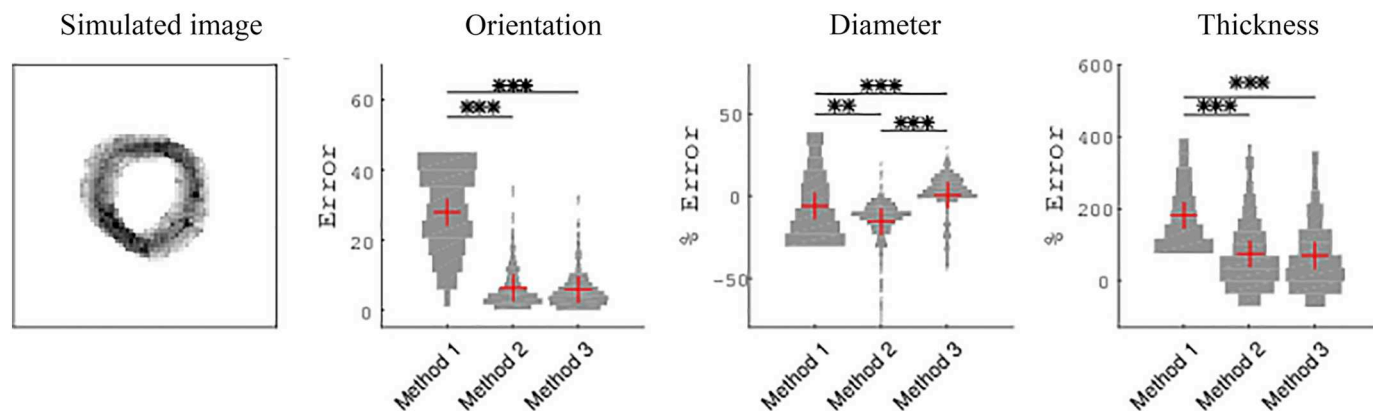


Fig. 3. An example of the simulated images of individual capillaries used for testing the performance of methods 1–3, and the errors obtained for each in estimating orientation (deviation angle in degrees), diameter and thickness (relative error). The significant differences between the methods (assessed by the Wilcoxon rank sum test) are indicated with star symbols: \* for  $p \leq 0.05$ , \*\* for  $p \leq 0.001$  and \*\*\* for  $p \leq 10^{-5}$ .

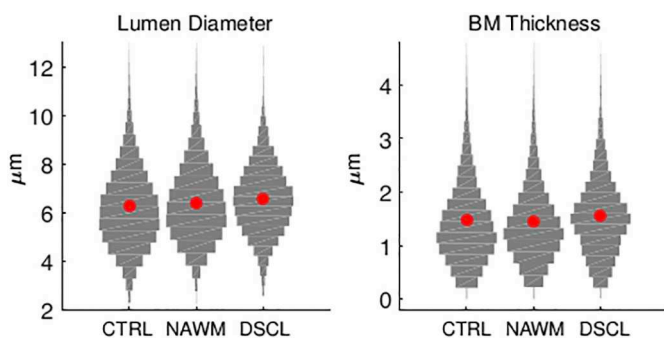


Fig. 4. Distribution of lumen diameters and BM thickness of individual capillaries estimated for each of the 3 population groups from 25 CTRL, 25 NAWM and 25 DSCL cases. The distributions include intra- and inter-subject variability.

aged mostly between 40 and 65 years old. The distribution of capillary diameters in deep white matter in Fig. 4,  $d \sim \mathcal{N}(6.26, 1.60)$ , is similar to the one reported by Cassot et al.,  $d \sim \mathcal{N}(6.46, 1.70)$ , from cerebral cortex. Another stereological study (Bouras et al., 2006) estimating capillary diameters from cortex and hippocampus, from 82 to 101 years old subjects, reported mean capillary diameters of 7.88  $\mu\text{m}$ , in their 4 control subjects in the hippocampus area CA1, and 7.38  $\mu\text{m}$  in the entorhinal cortex. The larger values in those brain regions compared to ours in deep white matter can be attributed to regional variability, and highlights the importance of not blindly extrapolating capillary characteristics from one region to another.

We observed an increase in the subject-specific mean capillary basement membrane thickness in DSCL, as shown in Fig. 5 and Table 2. Capillary basement membrane thickening has been previously reported in other brain regions (see Table 1) for aging patients (Riddle et al.,

2003) and patients with similar pathologies such as age related periventricular lesions (Cassot et al., 2006) and AD (Zlokovic, 2005). The biochemical mechanism(s) for basement membrane thickening are unclear. Age-related basement membrane thickening is caused by the deposition of collagen fibrils in and around the basement membrane (micro-vascular fibrosis) (Farkas et al., 2006). Some have suggested that fibrosis is induced in vascular dementia and AD by decreased cerebral blood flow (Farkas and Luiten, 2001). Our work, however, offers no conclusions regarding these mechanisms.

The intra-subject diameter standard deviation was significantly reduced in lesion ( $p < 0.001$ ), compared to NAWM and CTRL (Fig. 5). In addition, the capillary density was significantly decreased in lesions ( $p < 0.05$ ), compared to NAWM and CTRL. This reduction in the intra-subject variability and the capillary density, with the apparent increase (not statistically significant) of the lumen diameter mean, suggest that the capillaries with smallest diameters are decimated in DSCL. Capillary losses in aging and dementia subjects has been reported earlier (see Table 1). Also, losses in afferent vessels (arteries, arterioles and capillaries) have been reported in subjects with periventricular lesions (Moody et al., 2004). Losing capillaries in aging and dementia has been linked to the decline in the capacity of cerebral angiogenesis. However, capillary density from deep subcortical white matter and losses in DSCL had not been previously reported.

Our study provides two important evidences of microstructural changes which might explain the reduction of cerebral blood flow in age-related DSCLs observed with MRI. First, the increase in basement membrane thickness in DSCL compared to NAWM is usually correlated with an increase in the tortuosity of the vessels (Feigin, 2007), which leads to hypoperfusion (Brown, 2010) and, hence, reducing cerebral blood flow. Second, the decrease in capillary density also leads to a decrease in cerebral blood perfusion (Su et al., 2012). Impaired

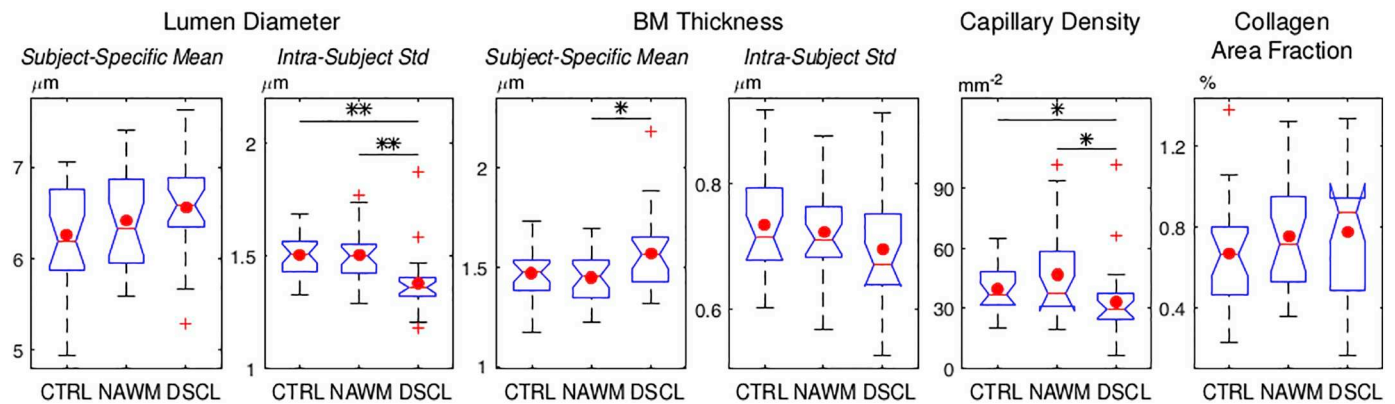


**Fig. 5.** Distribution of the subject-specific means and intra-subject variability of lumen diameter and BM thickness, and distribution of capillary density and collagen area fraction on the white matter surface cut. They are stratified according to the groups CTRL, NAWM, and DSCL. Each group displayed here has 25 samples of the parameters, obtained from the 25 subjects of each type. Significant differences between groups (Wilcoxon rank sum test) are indicated with star symbols: \* for  $p \leq 0.05$  and \*\* for  $p \leq 0.001$ .

**Table 2**

Statistics of 25 CTRL, 25 NAWM and 25 DSCL subjects. Diameters and thickness are expressed in  $\mu\text{m}$ , capillary density in  $\text{mm}^{-2}$ , and area fraction in %.

		CTRL	NAWM	DSCL	Global
Lumen diameter	Mean	6.26	6.41	6.55	6.41
	Intra-Subj. std	1.50	1.50	1.38	1.46
	Inter-Subj. std	0.60	0.53	0.50	0.56
	Total std	1.60	1.58	1.44	1.59
BM thickness	Mean	1.47	1.45	1.57	1.50
	Intra-Subj. std	0.73	0.72	0.70	0.72
	Inter-Subj. std	0.10	0.12	0.13	0.13
	Total std	0.75	0.73	0.72	0.74
Capillary density	Mean	39.9	46.7	33.0	39.9
	Inter-Subj. std	12.3	24.2	18.6	19.6
Collagen area fraction	Mean	0.67	0.76	0.77	0.74
	Inter-Subj. std	0.25	0.28	0.29	0.27

microcirculation could prevent responses to changes in metabolic demands, in patients with DSCLs, leading to cognitive impairment and dementia.

DSCLs are related with small vessel disease (SVD) and earlier MRI studies of cerebral blood flow also indicated vascular alterations in NAWM and DSCL (Marstrand et al., 2002; Brickman et al., 2009). However, quantitative microvascular changes associated with SVD in DSCL have not been reported. This work presents quantitative values of capillary microstructural manifestations of SVDs, which includes thickening and decrease in density, in brains with DSCL. This study indicate that the most severe changes due to SVDs occur at the site of DSCLs.

The statistics of capillary morphology changes reported here can be used in blood microcirculation modeling, for instance, for the development and validation of MRI techniques for microcirculation characterization (Mozumder et al., 2018). Further, the reduction of capillary density and increase in thickness in DSCL compared to NAWM, indicates that DSCLs could be potentially localized and clinically accessed using cerebral flow rates obtained with MRI. This can be useful for early diagnosis of DSCLs, opening the door to interventions that inhibit the progression or even revert white matter damage, such as exercising (Paillard, 2015; Chao et al., 2015) or drugs (Cho et al., 2006) showing promising results.

In contrast with previous evidences (Wharton et al., 2015) of abnormalities in NAWM regions in subjects with DSCL, we have not found significant differences between NAWM and CTRL. This cannot discard

the supposed field of abnormality around DSCL, but indicates that the any related capillary change is more subtle or more local than expected.

In this work, we also proposed a novel approach for the automatic estimation of capillary diameter and thickness from immunohistochemistry-labeled histology, robust to the orientation of the capillary regarding the image slice and to non-circularity of their cross sections. We tested three methods modeling capillaries with increasing levels of complexity, with synthetically generated capillary images. To avoid using the same models to generate the data, the synthetic images had higher level of complexity than the proposed methods, including irregular boundary shapes and changing radii along the capillary axial direction.

Method 1 is an automatic version of the approach followed by (Mancardi et al., 1980). Although simple and fast to compute, this method leads to large estimation errors, particularly in estimated thickness (Fig. 3). The tilted cylinders representing the microvasculature appear wider than expected; treating them as vertical cylinders introduces bias in the estimated thickness. The bias could be reduced by selecting only near-perpendicular capillaries. However, this drastically reduces the number of capillaries used in the analysis, decreasing their statistical significance. In addition, the estimation error would still be large, as shown in Supplementary Fig. 1. Method 2 used a more realistic model, modeling the capillary image as the projection of the intersection of the slice by a hollow cylinder with some inclination. Fig. 3 shows lower errors using Method 2. However, the diameter accuracy was still poor (mode around 10% error). This is possibly because most capillaries present severely distorted boundaries and assuming a circular cross section is insufficient. Method 3 further extended the cross-sectional model representing it with Fourier shape functions. Although its higher model complexity leads to longer estimation times, the diameter accuracy is improved (Fig. 3, and Supplementary Fig. 1). Introducing a further level of complexity, such as different shape coefficients for inner and outer diameters, would substantially increase the number of estimated parameters, possibly making the estimation problem ill-conditioned. The consequent increase in computational time would slow down the analysis of large datasets, as required in this work.

One limitation of this work is the shrinking of the samples caused by immersing them in fixative. No quantification of this effect is available in the literature, but the effect will be the same in all samples, and hence the relative differences observed would remain the same in absence of the shrinking. Also note that the reported statistics are obtained from an aging population ( $> 70$  years) and cannot be extrapolated to younger population without further studies.

DSCLs are discontinuous and might not appear in some MRI slices, unlike periventricular lesions which are more continuous. Hence, we

might have missed lesions during MRI and this could have led to some miscategorized NAWM as controls. However, the differences of DSCL with NAWM and controls (in capillary density and intra-subject std. of lumen diameter) is unaffected by this.

Future work will focus on realistic modeling of cerebral capillary flows using the distribution of capillary diameters and orientations obtained in this work. Using such simulations, we will explore the possibilities of detecting flow changes using MRI techniques for early diagnosis of age related deep WML.

## 5. Conclusion

To the best of our knowledge, this study is the first quantitative histomorphometric analysis of microvasculature in deep subcortical white matter. For the first time, we report specific microvascular changes in deep white matter regions with and without the presence of WMLs. Since WMLs are common in the aging brain, and a major cause of dementia in them, we studied an aging population of > 70 years. We estimated four microvascular features: lumen diameter, BM thickness, capillary density, and collagen area fraction, and reported their probability distributions in Control, NAWM, and DSCL groups. We found evidences of microstructural changes in DSCL leading to reduced blood flow: an increase in capillary thickness (leading to increase in tortuosity) and a decrease in capillary density. The statistically significant differences observed between the groups improves our understanding of the microvascular changes related to the blood flow reduction previously observed in DSCL and often assumed to be a cause factor. This is the most extensive and detailed histomorphometric analysis of capillary feature distributions, which will inform realistic models of cerebral blood flow and microstructural MRI models, potentially improving our understanding of white matter lesion progression and its diagnosis.

## Acknowledgments

Work supported by OCEAN Project (EP/M006328/1, PI: Prof. AF Frangi) and MedIAN Network (EP/N026993/1, PI: Prof. A Noble) funded by Engineering and Physical Sciences Research Council (EPSRC). Individual CFAS centers were supported by the UK NIHR Biomedical Research Centre for Ageing and Age – awarded to Newcastle-upon-Tyne Hospitals Foundation Trust; Cambridge Brain Bank supported by the NIHR Cambridge Biomedical Research Centre; Nottingham University Hospitals NHS Trust; University of Sheffield, Sheffield Teaching Hospitals NHS Foundation Trust and Sheffield NIHR Biomedical Research Centre; The Thomas Willis Oxford Brain Collection, supported by the Oxford Biomedical Research Centre; The Walton Centre NHS Foundation Trust, Liverpool. We acknowledge the essential contribution of liaison officers, general practitioners, their staff, and nursing and residential home staff. We are grateful to our respondents and their families for their generous gift to medical research, which has made this study possible. The Nanozoomer XR scanner was funded by the bet365/Denise Coates Foundation. The authors thank D Fillingham and L Baxter from SITraN, and L Beltrachini and M Raghavan-Sareena from CISTIB, for their help in the acquisition and processing of the digitized histology images and early discussions of this work.

## Appendix A. Supplementary data

Supplementary data to this article can be found online at <https://doi.org/10.1016/j.nicl.2019.101839>.

## References

Barber, R., Scheltens, P., Gholkar, A., Ballard, C., McKeith, I., Ince, P., Perry, R., Obrien, J., 1999. White matter lesions on magnetic resonance imaging in dementia with lewy bodies, Alzheimers disease, vascular dementia, and normal aging. *J. Neurol.*

- Neurosurg. Psychiatry 67 (1), 66–72.
- Bell, M.A., Ball, M., 1981. Morphometric comparison of hippocampal microvasculature in ageing and demented people: diameters and densities. *Acta Neuropathol.* 53 (4), 299–318.
- Bouras, C., Kovari, E., Herrmann, F.R., Rivara, C.-B., Bailey, T.L., von Gunten, A., Hof, P.R., Giannakopoulos, P., 2006. Stereologic analysis of microvascular morphology in the elderly: Alzheimer disease pathology and cognitive status. *J. Neuropathol. Exp. Neurol.* 65 (3), 235–244.
- Brayne, C., McCracken, C., Matthews, F.E., 2006. Cohort profile: the Medical Research Council cognitive function and ageing study (CFAS). *Int. J. Epidemiol.* 35, 1140–1145.
- Brickman, A.M., Zahra, A., Muraskin, J., Steffener, J., Holland, C.M., Habeck, C., Borogovac, A., Ramos, M.A., Brown, T.R., Asllani, I., et al., 2009. Reduction in cerebral blood flow in areas appearing as white matter hyperintensities on magnetic resonance imaging. *Psychiatry Res. Neuroimaging* 172 (2), 117–120.
- Brown, W.R., 2010. A review of string vessels or collapsed, empty basement membrane tubes. *J. Alzheimers Dis.* 21 (3), 725–739.
- Cassot, F., Lauwers, F., Fouard, C., Prohaska, S., Lauwers-Cances, V., 2006. A novel three-dimensional computer-assisted method for a quantitative study of microvascular networks of the human cerebral cortex. *Microcirculation* 13 (1), 1–18.
- Chao, F., Zhang, L., Luo, Y., Xiao, Q., Lv, F., He, Q., Zhou, C., Zhang, Y., Jiang, L., Jiang, R., et al., 2015. Running exercise reduces myelinated fiber loss in the dentate gyrus of the hippocampus in APP/PS1 transgenic mice. *Curr. Alzheimer Res.* 12 (4), 377–383.
- Cho, K.-O., La, H.O., Cho, Y.-J., Sung, K.-W., Kim, S.Y., 2006. Minocycline attenuates white matter damage in a rat model of chronic cerebral hypoperfusion. *J. Neurosci. Res.* 83 (2), 285–291.
- Claudio, L., 1995. Ultrastructural features of the blood-brain barrier in biopsy tissue from Alzheimer's disease patients. *Acta Neuropathol.* 91 (1), 6–14.
- Debette, S., Markus, H., 2010. The clinical importance of white matter hyperintensities on brain magnetic resonance imaging: systematic review and meta-analysis. *Br. Med. J.* 341, c3666.
- Deroulers, C., Ameisen, D., Badoual, M., Gerin, C., Granier, A., Lartaud, M., 2013. Analyzing huge pathology images with open source software. *Diagn. Pathol.* 8 (1), 92.
- Devine, M.E., Fonseca, J.A.S., Walker, Z., 2013. Do cerebral white matter lesions influence the rate of progression from mild cognitive impairment to dementia? *Int. Psychogeriatr.* 25 (1), 120–127.
- Duvernoy, H., Delon, S., Vannson, J., 1981. Cortical Blood Vessels of the Human Brain. vol. 7. pp. 179–519.
- Farkas, E., Luiten, P.G., 2001. Cerebral microvascular pathology in aging and Alzheimer's disease. *Prog. Neurobiol.* 64 (6), 575–611.
- Farkas, E., De Jong, G.I., De Vos, R.A., Steur, E.J., Luiten, P.G., 2000. Pathological features of cerebral cortical capillaries are doubled in alzheimers disease and parkinsons disease. *Acta Neuropathol.* 100 (4), 395–402.
- Farkas, E., de Vos, R.A., Donka, G., Jansen Steur, E.N., Mihály, A., Luiten, P.G., 2006. Age-related microvascular degeneration in the human cerebral periventricular white matter. *Acta Neuropathologica* 111 (2), 150–157.
- Feigin, V.L., 2007. Handbook of Clinical Neuroepidemiology. Nova Publishers.
- Fernando, M.S., O'Brien, J.T., Perry, R.H., English, P., Forster, G., McMeeekin, W., Slade, J.Y., Golkhar, A., Matthews, F.E., Barber, R., Kalaria, R.N., Ince, P.G., N. G. of MRC CFAS, 2004. Comparison of the pathology of cerebral white matter with post-mortem magnetic resonance imaging (MRI) in the elderly brain. *Neuropathol. Appl. Neurobiol.* 30 (4), 385–395.
- Fernando, M.S., Simpson, J.E., Matthews, F., Brayne, C., Lewis, C.E., Barber, R., Kalaria, R.N., Forster, G., Esteves, F., Wharton, S.B., et al., 2006. White matter lesions in an unselected cohort of the elderly: molecular pathology suggests origin from chronic hypoperfusion injury. *Stroke* 37 (6), 1391–1398.
- Fischer, V., Siddiqi, A., Yusufaly, Y., 1990. Altered angioarchitecture in selected areas of brains with Alzheimer's disease. *Acta Neuropathol.* 79 (6), 672–679.
- Foster, N.J., Sanderson, A.C., 1984. Determining object orientation from a single image using multiple information sources, Carnegie-Mellon University, Pittsburgh, PA, CMU-RI-TR-84-15.
- Gibbons, J.D., Chakraborti, S., 2011. Nonparametric statistical inference. In: International Encyclopedia of Statistical Science. Springer, pp. 977–979.
- Gundersen, H.J.G., Jensen, E.B., 1987. The efficiency of systematic sampling in stereology and its prediction. *J. Microsc.* 147 (3), 229–263.
- Gundersen, H., Boyce, R., Nyengaard, J., Odgaard, A., 1993. Bone morphometry 1992 sixth international congress proceedings the coneulor: unbiased estimation of connectivity using physical disectors under projection. *Bone* 14 (3), 217–222.
- Hoffmann, H., 2015. Violin. In: Simple Violin Plot Using MATLAB Default Kernel Density Estimation. vol. 5. INRES (University of Bonn), Katzen-burgweg, pp. 53115.
- Hunziker, O., Abdelal, S., Schulz, U., 1979. The aging human cerebral cortex: a stereological characterization of changes in the capillary net. *J. Gerontol.* 34 (3), 345–350.
- Kaipio, J., Somersalo, E., 2005. Statistical and Computational Inverse Problems. Springer, Newyork.
- Lagarias, J.C., Reeds, J.A., Wright, M.H., Wright, P.E., 1998. Convergence properties of the nelder-mead simplex method in low dimensions. *SIAM J. Optim.* 9 (1), 112–147.
- Lauwers, F., Cassot, F., Lauwers-Cances, V., Puwanarajah, P., Duvernoy, H., 2008. Morphometry of the human cerebral cortex micro-circulation: general characteristics and space-related profiles. *Neuroimage* 39 (3), 936–948.
- Lepelletier, F.-X., Mann, D., Robinson, A., Pinteaux, E., Boutin, H., 2017. Early changes in extracellular matrix in Alzheimer's disease. *Neuropathol. Appl. Neurobiol.* 43 (2), 167–182.
- Løkkegaard, A., Nyengaard, J.R., West, M.J., 2001. Stereological estimates of number and length of capillaries in subdivisions of the human hippocampal region. *Hippocampus* 11 (6), 726–740.
- Mancardi, G.L., Perdelli, F., Rivano, C., Leonardi, A., Bugiani, O., 1980. Thickening of the

- basement membrane of cortical capillaries in Alzheimer's disease. *Acta Neuropathol.* 49 (1), 79–83.
- Mann, D.M., Eaves, N.R., Marcyniuk, B., Yates, P.O., 1986. Quantitative changes in cerebral cortical microvasculature in ageing and dementia. *Neurobiol. Aging* 7 (5), 321–330.
- Marstrand, J., Garde, E., Rostrup, E., Ring, P., Rosenbaum, S., Mortensen, E.L., Larsson, H., 2002. Cerebral perfusion and cerebrovascular reactivity are reduced in white matter hyperintensities. *Stroke* 33 (4), 972–976.
- Massey Jr., F.J., 1951. The Kolmogorov-Smirnov test for goodness of fit. *J. Am. Stat. Assoc.* 46 (253), 68–78.
- Moody, D.M., Thore, C.R., Anstrom, J.A., Challa, V.R., Langefeld, C.D., Brown, W.R., 2004. Quantification of afferent vessels shows reduced brain vascular density in subjects with leukoaraiosis. *Radiology* 233 (3), 883–890.
- Mouton, P.R., Gokhale, A.M., Ward, N.L., West, M.J., 2002. Stereological length estimation using spherical probes. *J. Microsc.* 206 (1), 54–64.
- M. Mozumder, **Capillary Immunohistochemistry Images and Codes to Analyse them** doi:<https://doi.org/10.6084/m9.figshare.c.4132145.v1>, Accessed: 2018-13-06 (2018).
- Mozumder, M., Beltrachini, L., Collier, Q., Pozo, J.M., Frangi, A.F., 2018. Simultaneous magnetic resonance diffusion and pseudo-diffusion tensor imaging. *Magn. Reson. Med.* 79 (4), 2367–2378.
- Otsu, N., 1975. A threshold selection method from gray-level histograms. *Automatica* 11 (285–296), 23–27.
- Ovbiagele, B., Saver, J.L., 2006. Cerebral white matter hyperintensities on MRI: current concepts and therapeutic implications. *Cerebrovasc. Dis.* 22 (2–3), 83–90.
- Paillard, T., 2015. Preventive effects of regular physical exercise against cognitive decline and the risk of dementia with age advancement. *Sports Med. Open* 1 (1), 20.
- Park, K.H., Lee, J.-Y., Na, D.L., Kim, S.Y., Cheong, H.-K., Moon, S.Y., Shim, Y.S., Park, K.W., Ku, B.D., Choi, S.H., Joo, H., Lee, J.S., Go, S.M., Kim, S.H., Kim, S., Cha, K.R., Lee, J., Seo, S.W., 2011. Different associations of periventricular and deep white matter lesions with cognition, neuropsychiatric symptoms, and daily activities in dementia. *J. Geriatr. Psychiatry Neurol.* 24 (2), 84–90.
- Photonics, H., 2016. **Hamamatsu Photonics**. [www.hamamatsu.com/us/en/index.html](http://www.hamamatsu.com/us/en/index.html).
- Richard, E., 2010. **Vascular Factors in Dementia: Prevention and Pathology**. Ph.D. thesis. University of Amsterdam.
- Riddle, D.R., Sonntag, W.E., Lichtenwalner, R.J., 2003. Microvascular plasticity in aging. *Ageing Res. Rev.* 2 (2), 149–168.
- Ruifrok, A.C., Johnston, D.A., et al., 2001. Quantification of histochemical staining by color deconvolution. *Anal. Quant. Cytol. Histol.* 23 (4), 291–299.
- Scheltens, P., Barkhof, F., Leys, D., Pruvo, J., Nauta, J., Vermersch, P., Steinling, M., Valk, J., 1993. A semiquantitative rating scale for the assessment of signal hyperintensities on magnetic resonance imaging. *J. Neurol. Sci.* 114 (1), 7–12.
- Srivastava, K., Shah, R., Valia, D., Swaminarayan, H., 2013. Data mining using hierarchical agglomerative clustering algorithm in distributed cloud computing environment. *Int. J. Comp. Theor. Eng.* 5 (3), 520.
- Su, S.-W., Catherall, M., Payne, S., 2012. The influence of network structure on the transport of blood in the human cerebral microvasculature. *Microcirculation* 19 (2), 175–187.
- Thal, D.R., Ghebremedhin, E., Orantes, M., Wiestler, O.D., 2003. Vascular pathology in Alzheimer disease: correlation of cerebral amyloid angiopathy and arteriosclerosis/lipohyalinosis with cognitive decline. *J. Neuropathol. Exp. Neurol.* 62 (12), 1287–1301.
- Wharton, S.B., Simpson, J.E., Brayne, C., Ince, P.G., 2015. Age-associated white matter lesions: the mrc cognitive function and ageing study. *Brain Pathol.* 25 (1), 35–43.
- Zlokovic, B.V., 2005. Neurovascular mechanisms of Alzheimer's neurodegeneration. *Trends Neurosci.* 28 (4), 202–208.